HHS Public Access

Author manuscript

Neurobiol Dis. Author manuscript; available in PMC 2019 July 01.

Published in final edited form as:

Neurobiol Dis. 2018 July ; 115: 82–91. doi:10.1016/j.nbd.2018.04.006.

The KASH-containing isoform of Nesprin1 giant associates with ciliary rootlets of ependymal cells

C. Potter[1], **D. Razafsky**[1], **D. Wozniak**[2], **M. Casey**[1], **S. Penrose**[1], **X. Ge**[3], **M.R. Mahjoub**[4], and **D. Hodzic**[1,#,*]

[1]Department of Ophthalmology and Visual Sciences, Washington University School of Medicine, 660 S. Euclid Ave, St Louis, MO, 63110, USA

[2]Department of Psychiatry, Washington University School of Medicine, 660 S. Euclid Ave, St Louis, MO, 63110, USA

[3]Department of Radiology, Washington University School of Medicine, 660 S. Euclid Ave, St Louis, MO, 63110, USA

[4]Department of Medicine, Washington University School of Medicine, 660 S. Euclid Ave, St Louis, MO, 63110, USA

Abstract

Biallelic nonsense mutations of *SYNE1* underlie a variable array of cerebellar and non-cerebellar pathologies of unknown molecular etiology. *SYNE1* encodes multiple isoforms of Nesprin1 that associate with the nuclear envelope, with large cerebellar synapses and with ciliary rootlets of photoreceptors. Using two novel mouse models, we determined the expression pattern of Nesprin1 isoforms in the cerebellum whose integrity and functions are invariably affected by *SYNE1* mutations. We further show that a giant isoform of Nesprin1 associates with the ciliary rootlets of ependymal cells that line brain ventricles and establish that this giant ciliary isoform of Nesprin1 harbors a KASH domain. Whereas cerebellar phenotypes are not recapitulated in Nes1g$^{STOP/STOP}$ mice, these mice display a significant increase of ventricular volume. Together, these data fuel novel hypotheses about the molecular pathogenesis of *SYNE1* mutations and support that KASH proteins may localize beyond the nuclear envelope *in vivo*.

[#]**CORRESPONDING AUTHOR**, *Present address: Washington University School of Medicine, Department of Developmental Biology, Campus Box 8103, 660 S. Euclid Ave, St Louis, MO, 63110, USA. dhodzic@wustl.edu, Phone: 314-273-3051, ORCID ID: 0000-0002-2113-8936.

[*]Present address: Washington University School of Medicine, Department of Developmental Biology, 660 S. Euclid Ave, St Louis, MO, 63110, USA.

AUTHOR CONTRIBUTIONS

Conceptualization, D.H.; Formal analysis: D.W., X.G., D.H.; Methodology: D.W., X.G., D.H.; Investigation: C.P., D.W., D.R., M.C., S.P., D.H.; Resources: D.H., M.R.M.; Writing-original draft: D.H.; Writing-review & editing; D.W., M.R.M., D.R., X.G.; Visualization: D.H.; Supervision: D.H.; Project administration: D.H.; Funding acquisition: D.H.

Keywords

SYNE1; Nesprin1; ciliary rootlets; cerebellar ataxia; ARCA1; SCAR8; ependymal cells; brain ventricles; KASH

INTRODUCTION

Nesprins (Nuclear envelope spectrin repeats) correspond to a family of nuclear envelope (NE) proteins encoded by five distinct mammalian genes (*SYNE1* to *5*). The molecular signature of all Nesprins corresponds to an evolutionary-conserved C-terminal KASH (Klarsicht/ANC1/Syne Homology) domain that consists of a transmembrane domain followed by a stretch of ~50 amino acids that tethers Nesprins to the NE (Starr and Han, 2002; Zhang et al., 2001). Within the perinuclear lumen that separates the outer nuclear membrane (ONM) from the inner nuclear membrane (INM), the luminal region of the KASH domain (~30 amino acids) interacts directly with the SUN (Sad1/UNC84) domain, the molecular signature of a family of INM proteins called Sun proteins (Haque et al., 2006; Hodzic et al., 2004; Padmakumar et al., 2005; Sosa et al., 2012; Zhou et al., 2012). Because multiple genes also encode Sun proteins, SUN/KASH interactions bring together various combinations of Nesprins and Sun proteins termed "Linkers of the Nucleoskeleton and the Cytoskeleton" (LINC complexes) at the NE (Crisp et al., 2006).

In 2007, biallelic nonsense mutations scattered across *SYNE1* (a majority of which are compound mutations) were genetically linked to Autosomal Recessive Cerebellar Ataxia type I (ARCA1) in a large cohort of patients from Quebec (Gros-Louis et al., 2007). This late-onset neurodegenerative pathology consists of a progressive limb and gait ataxia, dysarthria and severe cerebellar atrophy with no brain stem involvement (Gros-Louis et al., 2007; Izumi et al., 2013; Noreau et al., 2013). Because ARCA1 nonsense mutations span the coding sequence of Nesprin1 giant (Fig.1A) and underlie common clinical phenotypes, these studies suggested that ARCA1 is associated with the loss-of-function of large isoforms of Nesprin1. Using next generation sequencing on unbiased cohorts of more than 400 patients with idiopathic ataxic features, Synofzik et al. recently identified biallelic nonsense *SYNE1* mutations in more than 5% of ataxic individuals (Mademan et al., 2016; Synofzik et al., 2016). Importantly, a majority of patients displayed a wide array of multisystemic pathologies in addition to the typical ARCA1 phenotype. These pathologies consist of variable combinations of upper or lower motor neuron dysfunction, muscle atrophy and spasticity, scoliosis and kyphosis, cognitive disorders and respiratory distress (Mademan et al., 2016; Ozoguz et al., 2015; Synofzik et al., 2016; Wiethoff et al., 2016). These patients are now classified as cerebellar ataxia "plus" (CA+) by contrast to ARCA1 patients who are referred to as pure cerebellar ataxia (pCA) (Synofzik et al., 2016).

With more than 140 exons, *SYNE1* is a gigantic and complex gene that encodes multiple Nesprin1 isoforms such as Nesprin1α (~120 kDa), Nesprin1β (~350 kDa) and Nesprin1giant (Nes1g, ~1MDa) (Kobayashi et al., 2006; Loebrich et al., 2016; Marme et al., 2008; Simpson and Roberts, 2008; Zhang et al., 2002) (Fig.1A). The large size and partial overlap of coding sequences represent a significant challenge to establish the expression

pattern of these isoforms *in vivo*. This issue needs to be addressed since the position of biallelic compound mutations along *SYNE1* have the potential to affect distinct sets of Nesprin1 isoforms. Understanding the molecular pathogenesis of *SYNE1* mutations also requires more investigation of the biological functions of Nesprin1 isoforms. Indeed, whereas Nesprin1 isoforms that associate with the NE are well known for their function in nuclear positioning (Zhang et al., 2009; Zhang et al., 2007b), we recently identified a KASH-LESS variant of Nesprin1 giant (KLNes1g) that localizes to essential cerebellar synapses between afferent mossy fibers (MF) and cerebellar granule neurons (CGN) within the granule cell layer (GCL) (Razafsky and Hodzic, 2015). More recently, we also determined that Nesprin1α localizes at the ciliary rootlets of photoreceptors through its interaction with the N-terminal region of rootletin, the main components of ciliary rootlets (Potter et al., 2017). In this work, we developed two novel mouse models to untangle the expression pattern of *Syne1* in the cerebellum, show that the KASH-containing isoform of Nesprin1 giant localize to ciliary rootlets of ependymal cells and that its depletion correlates to a significant enlargement of the ventricular system. We also provide the first formal evidence that KASH domains also localize beyond the NE *in vivo*.

RESULTS

The expression of giant isoforms of Nesprin1 is specifically abrogated in Nes1g$^{STOP/STOP}$ mice

To specifically inhibit the expression of giant isoforms of Nesprin1, 16 bases including STOP codons in all reading frames and an EcoRI restriction site were inserted within exon -64 of *Syne1* used a CRISPR/Cas9 approach (Fig.1A, 1B). Targeting this exon was motivated by the high frequency of nonsense mutations within the corresponding region of *SYNE1* in ARCA1 patients (Dupre et al., 2007). In addition, this genetic alteration was not predicted to affect the coding sequence of Nesprin1α and Nesprin1β that are both encoded by downstream exons (Fig.1A). Genotyping identified one homozygous founder carrying the desired 16 bases insertion (Fig.1B). Sequencing of genotyping products from F2 mice identified a Q5328X nonsense mutation predicted to either truncate or suppress the expression of both Nes1g and KLNes1g. This strain, that we named *Nes1g*$^{STOP/STOP}$, was fertile and undistinguishable by size or weight from *Nes1g*$^{STOP/WT}$ littermates.

Immunoblotting of cerebellar and brain lysates from *Nes1g*$^{STOP/STOP}$, *Nes1g*$^{STOP/WT}$ and *Nes1g*$^{wt/wt}$ littermates with the Nes1HAA12 antibody, whose epitope overlaps with the coding sequences of all Nesprin1 isoforms (Fig.1A), showed that giant isoforms of Nesprin1 (~1MDa) were depleted from *Nes1g*$^{STOP/STOP}$ lysates (Fig.1C, left panel and Fig.S1A). Immunoblotting with Nes1QFA13, whose epitope is located upstream from the Q5328X mutation (Fig.1A), confirmed the complete depletion of giant isoforms of Nesprin1 in *Nes1g*$^{STOP/STOP}$ brains (Fig.1C, right panel) and did not emphasize any truncated protein that may have resulted from the introduction of the Q5328X mutation (Fig.1C, right and Fig.S1A). Note that even though lysates separated on polyacrylamide gels provide the same qualitative results (Fig.S1A), vertical agarose gel electrophoresis is best suited to unequivocally resolve large isoforms of Nesprin1. Together, these results indicated that *Nes1g*$^{STOP/STOP}$ mice are null for the expression of giant isoforms of Nesprin1.

Expression pattern of Nesprin1 isoforms in the cerebellum

KLNes1g is abundantly expressed at MF/CGN synapses scattered across the GCL (Razafsky and Hodzic, 2015). In agreement with the loss of giant isoforms of Nesprin1 in cerebellar lysates of *Nes1g*$^{STOP/STOP}$ mice, KLNes1g was undetectable in the GCL of *Nes1g*$^{STOP/STOP}$ cerebella whereas it localized to numerous patches, which correspond to MF/CGN synapses, in the GCL of *Nes1g*$^{STOP/WT}$ mice (Fig.1D, yellow arrows, Fig.S1B and S2A). A canonical Nesprin1 immunoreactivity detected at the NE *Nes1g*$^{STOP/WT}$ Bergmann glial cells (Fig.1D, red arrowheads and Fig.S1B) was also absent in *Nes1g*$^{STOP/STOP}$ cerebella suggesting that Nes1g exclusively decorates the NE of these cells. By contrast, the immunoreactivity of Nesprin1 at the NE of Purkinje cells was unaffected in *Nes1g*$^{STOP/STOP}$ mice (Fig.1D, yellow arrowheads, Fig.S1B and S2A). Similarly, immunostaining of *Nes1g*$^{STOP/STOP}$ cerebral cortex and hippocampus did not emphasize any obvious difference either in the intensity or the distribution of Nesprin1 rim-like patterns by comparison to *Nes1g*$^{STOP/WT}$ (Fig.S2B). These results suggested that smaller isoforms of Nesprin1 contribute most of the Nesprin1 immunoreactivity at the NE of Purkinje cells, cortical and hippocampal neurons. In the case of Purkinje cells, this isoform most likely corresponds to Nesprin1β for the following reasons: 1) in agreement with our genetic strategy that specifically targets giant isoforms of Nesprin1, a smaller immunoreactive bands corresponding to the molecular weight of Nesprin1β ~350 kDa was detected in *Nes1g*$^{STOP/STOP}$ cerebellar lysates with the Nes1HAA12 antibody but not with the QFA13 antibody (Fig.1C and Fig.S1A) whose epitope localizes upstream from the coding sequences of Nesprin1β (Fig.1A), 2) this ~350 kDa protein was specifically decreased in ^{ActinCre}Nesprin1$^{\Delta/\Delta}$ cerebellar lysates (Fig.1E) in which all isoforms of Nesprin1 are conditionally inactivated through the floxing of exon-16 (Fig.1A and (Razafsky and Hodzic, 2015)), 3) the expression of Nesprin1α is mostly restricted to skeletal muscle, heart and retina (Duong et al., 2014; Potter et al., 2017). Taken together, these data indicate that KLNes1g is expressed at MF/CGN synapses in the GCL, Nes1g at the NE of the Bergmann glia and Nesprin1β at the NE of Purkinje cells.

A giant isoform of Nesprin1 localizes to ciliary rootlets of ependymal cells

We recently reported that Nesprin1α associate with the ciliary rootlets of photoreceptors and predicted that larger isoforms may localize at ciliary rootlets of ependymal cells (Potter et al., 2017). Accordingly, patches of Nesprin1 immunoreactivity labeled *NES1g*$^{STOP/WT}$ ependymal ciliary rootlets (Fig.2A, left, yellow arrow). By contrast, this signal was undetectable in ependymal cells from *NES1g*$^{STOP/STOP}$ brains (Fig. 2A, right) suggesting that a large isoform of Nesprin1 associated with the base of cilia in ependymal cells. A side view of the ventricular surface provided by 200 μm-thick cerebral slices (Fig. S3A) further emphasized that Nesprin1 patches are distinct from ependymal cell nuclei (Fig.2B). Note that the NE of ependymal cells displayed a discontinuous distribution of Nesprin1 that appeared as NE linear aggregates (Fig.S3B). The expression of large isoforms of Nesprin1 in ependymal cells was further corroborated by strong *in situ* hybridization signals (Fig.2C) with three probes overlapping with the N-terminal (Nes1 ABD), central (Nes1 MID) or C-terminal (Nes1 KASH) region of giant *Syne1* transcripts (Fig.1A). Note that the Human protein atlas reports a strong Nesprin1 staining at the base of motile cilia in other multiciliated epithelia, such as those lining the Fallopian tubes and airways (https://www.proteinatlas.org, (Uhlen et al., 2015)). These results therefore indicate that in addition

to Nesprin1α, which associates with ciliary rootlets of photoreceptors (Potter et al., 2017), giant isoforms of Nesprin1 are recruited to ciliary rootlets of ependymal cells.

In vivo evidence that ciliary Nesprin1 isoforms harbor a KASH domain

The alternative splicing of exon-2 of *Syne1* results in a reading frameshift of exon-1 and determines whether Nesprin1 isoforms are synthesized either as KASH-containing or KASH-LESS isoforms (Fig.3A, top) (Razafsky et al., 2013). Interestingly, despite its localization at photoreceptor ciliary rootlets, i.e., beyond the NE, we previously showed that Nesprin1α is exclusively encoded by transcripts that all included exon-2, i.e., by transcripts that lead to the exclusive synthesis of KASH-containing Nesprin1α (Potter et al., 2017). This was significant as it suggested that KASH domain-containing proteins may also localize outside the NE. However, these data did not exclude that ciliary Nesprin1 may also originate either from another premature STOP codon due to the alternative splicing of additional upstream exons or still from a proteolytic cleavage that would remove the KASH domain of ciliary Nesprins. Because no antibody currently allows for the specific detection of the KASH domain of Nesprin1, we developed a "KASH reporter" mouse model where a 3XFLAG tag followed by a STOP codon (3XFLAG/STOP) was inserted within exon-1 both upstream and in frame with the coding sequence of the KASH domain of *Syne1* (Fig.3A, bottom). As such, *Syne1* transcripts containing exon-2 solely encode FLAG-tagged versions of natural isoforms of Nesprin1 in which the KASH domain is replaced by a 3XFLAG C-terminal tag. By contrast, transcripts lacking exon-2 still encode the natural C-terminal sequence of KASH-LESS isoforms of Nesprin1 (Fig.3A, bottom). As shown in Figure 3B, immunoblotting of $Nes1^{FLAG/FLAG}$ and $Nes1^{FLAG/WT}$ cerebral lysates either with Nesprin1 or FLAG antibodies emphasized FLAG-tagged bands that co-migrated with Nes1g. In agreement with the identification of the ~350 kDa band as Nesprin1β (Fig. 1E), this band was effectively flag-tagged (Fig.3B). Brain slices from $Nes1^{FLAG/WT}$ were immunostained with the FLAGM2 antibody. As shown in Figure 3C, a robust FLAG immunoreactivity colocalized both with NES1HAA12 (left panel) and rootletin (right panel) at ciliary rootlets of $Nes1^{FLAG/WT}$ ependymal cells. Similar experiments performed with $Nes1^{FLAG/WT}$ retinas further emphasized that Nesprin1α (~120 kDa) was also FLAG-tagged (Fig.3D) and that a FLAGM2 immunoreactivity colocalized with rootletin at ciliary rootlets that line the inner segment of photoreceptors (Fig.3E). In agreement with our previous *in vitro* experiments (Potter et al., 2017) showing that the KASH domain is dispensable for the interaction of Nesprin1α with rootletin, these data show that the KASH domain is dispensable for the ciliary localization of giant isoforms of Nesprin1 *in vivo*. They also show that the ciliary localization of Nesprin1 does not originate from upstream premature STOP codon or proteolytic cleavage that would remove the C-terminal KASH domain, in which case we would not detect the FLAG immunoreactivity at ciliary rootlets. These results further fuel the idea that KASH isoforms of Nesprin1 also localize to ciliary rootlets in addition to the NE.

Phenotypical analyses of $NES1g^{STOP/STOP}$ mice

A common phenotype of all patients affected by *SYNE1* mutations consists of a severe atrophy of the cerebellum (Gros-Louis et al., 2007; Synofzik et al., 2016). However, P25 and 1 year-old $Nes1g^{STOP/STOP}$ cerebella did not display any obvious anatomical disorganization

and the density of Purkinje cells as well as the overall thickness of the GCL were similar to *Nes1g*$^{STOP/WT}$ cerebella (Fig.4A, Fig.S2A and data not shown). To strictly evaluate cerebellar volumes *in vivo*, *Nes1g*$^{STOP/STOP}$ and *Nes1g*$^{WT/WT}$ brains were imaged by MRI. Segmentation of MRI scans (see Material and Methods) did not reveal any atrophy of *Nes1g*$^{STOP/STOP}$ cerebella (Fig.4B and data not shown). Because carriers of *SYNE1* mutations are progressively affected by movement disorders, 1 year-old *Nes1g*$^{STOP/STOP}$ mice were also evaluated on a battery of sensorimotor tests designed to assess initiation of movement (walking initiation), balance (ledge and platform), coordination (pole and inclined screens), and strength (inverted screen) (Grady et al., 2006; Idol et al., 2014; Wozniak et al., 2004). These test failed to reveal any significant motor deficit in *Nes1g*$^{STOP/STOP}$ mice (Fig.4C). Taken together, these results indicate that the expression of large isoforms of Nesprin1 are dispensable both for the development and the homeostasis of the mouse cerebellum up to one year of age. Whereas cerebellar volumes were not affected, segmentation of different brain compartments of 1 year-old *NES1g*$^{STOP/STOP}$ mice revealed a striking enlargement of the ventricular lumen (Fig.4D, left). In light of our findings that Nes1g associates with the ciliary rootlets of ependymal cells, we repeated MRI experiments on three pairs of ~3 months-old *Nes1g*$^{STOP/STOP}$ and *Nes1g*$^{STOP/WT}$ littermates. Segmentation confirmed that the ventricular volume of *NES1g*$^{STOP/STOP}$ brains was significantly increased (Fig.4D, right). The correlation between the genetic ablation of Nes1g at ciliary rootlets of ependymal and a significant enlargement of the ventricular lumen suggest that multiciliated epithelia may be affected by *SYNE1* mutations and potentially underlie at least some of the non-cerebellar pathologies observed in *SYNE1* patients.

DISCUSSION

Despite an increasing number of reports linking mutations of *SYNE1* to a wide array of neurodegenerative (Gros-Louis et al., 2007; Izumi et al., 2013; Mademan et al., 2016; Noreau et al., 2013; Ozoguz et al., 2015; Synofzik et al., 2016; Wiethoff et al., 2016; Yoshinaga et al., 2017; Yucesan et al., 2017) and neuromuscular pathologies (Attali et al., 2009; Baumann et al., 2017; Fanin et al., 2015; Laquerriere et al., 2014; Wu et al., 2017; Zhang et al., 2007a), the molecular pathogenesis of *SYNE1* mutations remains obscure. This is in part due to the challenge of determining which isoform(s) are expressed in various cell types. In this work, we show that KLNes1g is expressed at MF/CGN synapses in the GCL, Nes1g at the NE of the Bergmann glia and Nesprin1β at the NE of Purkinje cells. Since all biallelic truncations of *SYNE1* invariably affect the coding sequence of both Nes1g and KLNes1g and are all linked to a loss of integrity and function of the cerebellum, our data suggest that the cerebellar symptoms of *SYNE1* patients originate from a progressive dysfunction of MF/GCN synapses and/or of the Bergmann glia. In addition, *SYNE1* patients harboring biallelic nonsense mutations that that both fall within the coding sequence of Nesprin1β may display additional cerebellar dysfunctions due to the additional loss of expression of Nesprin1β at the NE of Purkinje cells. In fact, biallelic truncations of Nesprin1β may affect many other tissues as this isoform appears to be ubiquitously expressed. Indeed, Nesprin1α expression is mostly restricted to the retina, heart and skeletal muscle (Duong et al., 2014; Potter et al., 2017) and the lack of expression of Nes1g and KLNes1g did not obviously affect the Nesprin1 immunoreactivity at the NE of major cell

types of the cortex and the hippocampus. In agreement with these observations, DNase I hypersensitivity profiling of *SYNE1* suggest that the Nesprin1β promoter is active in a vast majority of adult mouse tissues (Fig. S4). Together, these data provide the first detailed expression pattern of multiple isoforms of Nesprin1 in the cerebellum. They also suggest that biallelic mutations that both fall within the coding sequence of Nesprin1β may result in more complex and/or severe clinical outcomes by comparison to biallelic mutations that solely affect the expression of giant isoforms of Nesprin1 (Razafsky and Hodzic, 2015). Accordingly, Wiethoff et al. reported that mutations located nearer to the 3' end of *SYNE1* were more frequently associated with motor neuron or neuromuscular involvement (Wiethoff et al., 2016). By the same token, a genotype-phenotype analysis of the cohort of patients described by Synofzik et al. (Synofzik et al., 2016) also suggest that biallelic mutations of *SYNE1* that both fall within the coding sequence of Nesprin1β most often lead to more complex clinical presentations (data not shown). In addition to the genetic linkage of Arthrogryposis Multiplex Congenita with biallelic mutations affecting the coding sequence of Nesprin1α (Attali et al., 2009; Baumann et al., 2017), it appears that a genotype-phenotype correlation starts to emerge for *SYNE1* pathologies.

Except for the enlargement of the ventricular system, Nes1g$^{STOP/STOP}$ mice did not display any obvious phenotype. Similarly, mice harboring a truncation of the N-terminal actin-binding domain of Nes1g (Fig.1A) appeared normal (Stroud et al., 2017). Since there is ample genetic evidence that biallelic mutations of giant isoforms of Nesprin1 underlie cerebellar pathologies in humans (Gros-Louis et al., 2007; Izumi et al., 2013; Mademan et al., 2016; Synofzik et al., 2016; Wiethoff et al., 2016), the lack of anatomical and behavioral phenotype of *Nes1g*$^{STOP/STOP}$ mice suggest that either the C57/Bl6 strain or mice in general may not be the appropriate organism to model cerebellar phenotypes resulting from *SYNE1* mutations. Alternatively, *Nes1g*$^{STOP/STOP}$ should be examined at later time points but behavioral studies may be affected by aging phenotypes to draw any significant conclusion.

Our poor understanding of the molecular pathogenesis of *SYNE1* mutations also stems from mounting evidence that Nesprin1 isoforms also play essential biological roles beyond the NE. Indeed, KLNes1g is abundantly expressed at MF/GCN synapses and Nesprin1α is recruited to photoreceptor ciliary rootlets (Potter et al., 2017; Razafsky and Hodzic, 2015). In this work, we show that Nes1g is recruited at the ciliary rootlets of ependymal cells and that its depletion is correlated to a significant increase of the ventricular volume. Since the cytoplasmic region of Nesprin1α, which corresponds to the C-terminal region of Nes1g (Fig.1A), mediates the interaction with rootletin (Potter et al., 2017), we hypothesize that biallelic truncations of *SYNE1* impair the recruitment of truncated Nes1g at the ciliary rootlets of ependymal cells. Alternatively, Nes1g may not be synthesized at all thereby also affecting the composition of ependymal ciliary rootlets in *SYNE1* patients. Note that whereas the functional inactivation of ciliary Nesprin1α requires the rare occurrence of biallelic mutations that would both fall within its coding sequence (Fig.1A) ((Baumann et al., 2017) and references therein), the functional inactivation of Nes1g at ciliary rootlets of ependymal cells is most likely a common occurrence since any combination of biallelic mutations of *SYNE1* is predicted to invariably affect giant isoforms of Nesprin1.

Using FLAG-tagged alleles of *Syne1*, we show that the KASH domain is dispensable for the localization of Nesprin1α and Nesprin1 giant at ciliary rootlets of photoreceptors and ependymal cells, respectively. This is in agreement with our previous biochemical data indicating that the KASH domain is dispensable for the interaction of Nesprin1α with rootletin. In addition, these data and our previous results strongly support the idea that ciliary Nesprin1 isoforms harbor a KASH domain. Indeed, 1) the detection of a FLAG immunoreactivity at ciliary rootlets of $Nes1^{FLAG/WT}$ (and $Nes1^{FLAG/FLAG}$, data not shown) indicates that the cytoplasmic region of ciliary Nesprin1 isoforms is not subjected to a proteolytic cleavage that would remove the KASH domain *in vivo*; 2) in photoreceptors, ciliary Nesprin1α is exclusively encoded by exon-2-containing transcripts that encode a KASH domain (Potter et al., 2017); 3) in cultured cells, recombinant EGFP-Nesprin1α is abundantly recruited to recombinant filaments of rootletin that accumulate at the centrosome (Potter et al., 2017). Taken together, these observations strongly support that KASH-containing isoforms of Nesprin1 also localize beyond the NE. Interestingly, several instances of Nesprin localization outside the NE have been reported in mammalian and fly skeletal muscles (Volk, 2013; Zhang et al., 2001). It will be important to examine whether these proteins also harbor a KASH domain. Because the KASH domain includes a transmembrane domain, it must be inserted in cellular membranes. Whereas photoreceptors ciliary rootlets are surrounded by a dense network of membranes (Yang et al., 2002), it remains to be determined whether ciliary rootlets of ependymal cells provide a similar environment that may allow for the insertion of the KASH domain in biological membranes.

Together, our data suggest that biallelic mutations of *SYNE1* may affect the function of ependymal cells lining the ventricular system in addition to cerebellar functions but the involvement of multiple isoforms of Nesprin1 in ciliary function remains to be strictly established. However, it is interesting to note that scoliosis, mental retardation and respiratory dysfunction, which are commonly associated with ciliary defects, have been reported in a subset of *SYNE1* patients (Baumann et al., 2017; Synofzik et al., 2016). For these reasons, we suggest that *SYNE1* mutations may potentially underlie ciliary defects in addition to cerebellar phenotypes.

MATERIAL AND METHODS

Animal models

Animal protocols used in this study strictly adhered to the ethical and sensitive care and use of animals in research and were approved by the Washington University School of Medicine Animal Studies Committee (Animal Welfare Insurance Permit #A-3381-01, protocol#20160171). $Nes1g^{STOP/STOP}$ and $Nes1^{FLAG/FLAG}$ mice (C57/Bl6 background) were generated using CRISPR-Cas9 as recently described (Yang et al., 2014). To generate $Nes1g^{STOP/STOP}$ mice, the guide sequence GTCTTGGGTTCAAGAAACGA and oligo sequence

AAAGTGAAGAATCATGGCAAGCTGGTAAAGCAGGAGCTCCAAGAACGGGAAGCAG

TGGAGACTCGTATTAACTCTGTGAAGTCTTGGGTT*TA*<u>*GAATTC*</u>*TAAGCTAA*CAAGAA

ACGAAGGACTATTTAGGGAATCCAACAATAGAGATCGACACACAACTAGAAGAAC T GAAGGTGCTCCTCTGAATTTGT were used (sequence in italic corresponds to inserted STOP codons in all reading frames and an EcoRI restriction site (underlined)). Nes1g$^{STOP/STOP}$ mice were genotyped with forward primer 5'-CTGCTTTCTCCCTCTGGTATTT -3' (F1) and reverse primer 5'-GAGCACCTTCAGTTCTTCTAGTT-3' (R1). To generate Nes1 $^{FLAG/FLAG}$ mice, the guide sequence ATTCCTCCCGTTCTGACCCC and the oligo sequence TGAGTTGTTTATGTCAATTCTTCCCTTAGGTCCACAAGAGATGGCTCCGATTCCTC C CGTTCT*GACTACAAAGACCATGACGGTGATTATAAAGATCATGACATCGACTACAA GGATGACGATGACAAG*TGACCCCAGGCCAGAACGGGTGGGTCGAGCCTTCCTGT TCCGGATCCTCCGGGCAGCTCTTC were used (sequence in italic corresponds to the 66 bases encoding the 3XFLAG epitope). Nes1 $^{FLAG/FLAG}$ mice were genotyped with forward primer 5'-TATCTCGGTGGTTGGGAAATG-3' (F1503) and reverse primer 5'-AAGGCAGGTGAGTCCAATAAG-3' (R1504).

Tissue lysate preparation and immunoblotting procedures

Mouse tissues were grinded in gel loading buffer (8M Urea, 2M thiourea, 3% SDS, 75mM DTT, 0.03% bromophenol blue, 50mM Tris (pH 6.8)) using a Bullet Blender and centrifuged at 12,000g for 10 min. Supernatants were heated at 60°C for 15 min and analyzed by Vertical Agarose Gel Electrophoresis as described by Warren et al. (Warren et al., 2003). After gel transfer, nitrocellulose membranes were stained with Ponceau S to label Titin, Nebulin and Myosin from skeletal muscle lysates, blocked with 5% milk in TBST (10mM Tris, 150mM NaCl, 0.1% Tween 20 (pH 7.3)) for 1 hour at room temperature and incubated overnight at 4°C with the primary antibodies. After washing with TBST, membranes were incubated with the appropriate HRP-conjugated secondary antibodies. Signals were detected using SuperSignal® West Pico solutions (Thermofisher) and exposed on x-ray film and/or imaged for quantification purposes on a G:Box HR16 imaging system (Syngene). For SDS-PAGE analysis, the same procedure was followed except that tissue lysates were loaded on precast 4–15% polyacrylamide gels (Biorad).

Immunofluorescence microscopy

Brains, retinas and skeletal muscle fibers were isolated from mice processed for transcardial perfusion with 4% PFA as previously described (Razafsky et al., 2015). Dissected tissues were either embedded in OCT to obtain 15 μm cryostat sections or embedded in 4% melting agarose and sectioned at 200 μm with a vibratome (VT1000S, Leica). For rootletin antibodies that require methanol fixation, mice were euthanized by C02 inhalation and 200 μm-thick vibratome slices were fixed in methanol at −20°C for 30 min. After fixation, PFA- or methanol-fixed tissues were processed for immunofluorescence as previously described in details (Razafsky et al., 2015). Briefly, sections in 24-well plates were rinsed three times in PBS, permeabilized in blocking buffer (10% donkey serum/0.5% Triton X-100 in PBS) for 30 min and incubated overnight with primary antibodies diluted in blocking buffer. After several washes with PBS, sections were incubated with secondary antibodies (Alexa 488 and 594, Thermofisher) for 1 h in blocking buffer. After several washes in PBS and DAPI staining, slices were mounted in anti-fading mounting medium (DAKO).

Image acquisition (single, large scans and *Z*-stacks) was performed with a Nikon Eclipse Ti coupled to a Coolsnap HQ2 (Photometrics) and an LED light source (Lumencor) with the NIS element software package (Nikon) with either 20× (n.a 1.0) or 40× (n.a. 1.4) objectives.

In situ hybridization

ISH was performed on mouse brain sections using the RNAscope 2.0 Red Kit (Advanced Cell Diagnostics) as previously described in details (Razafsky and Hodzic, 2015).

Antibodies

Nes1HAA12 and Nes1QFA13 antibodies were raised as previously described (Chambliss et al., 2013; Potter et al., 2017; Razafsky et al., 2013). Rootletin, Lamin B1, FLAGM2 and α-tubulin antibodies were purchased from Santa Cruz (#SC-67824, #SC-6216) and Sigma-Aldrich (#F3165, #T6199), respectively.

Magnetic resonance imaging

MRI experiments employed a 4.7-T small-animal MR scanner equipped with an Agilent/Varian (Santa Clara, CA) DirectDrive™ console and an Oxford Instruments (Oxford, United Kingdom) horizontal superconducting magnet with a 40-cm clear bore diameter. Data were collected with a laboratory-built, actively-decoupled transmit and receive coil pair: 7.5-cm ID volume transmitter coil, 1.8-cm OD surface receiver coil. Mice were placed on a warm-water pad and anesthetized with isoflurane/O_2 (1.2% isoflurane) throughout the experiment. Respiratory rate and core body temperature (rectal probe) were monitored with a Small Animal Instruments (Stony Brook, NY) monitoring and gating unit. T2-weighted transaxial images were collected with a 2D fast spin-echo multi-slice (FSEMS) sequence: 24 slices, echo train length 4, kzero 4, TR 3 s, effective TE 100 ms; matrix size 128 × 128, field of view (FOV) 16 × 16 mm^2, slice thickness 0.5 mm, 4 averages. The T1-weighted images were collected with a 3D gradient echo (GE3D) sequence: flip angle 30°, TR 30 ms, TE 2.2 ms, 0.19 mm isotropic resolution, FOV 24 × 24 × 24 mm^3, 2 averages. For data analysis, the T1W and T2W images were loaded into MatLab (MathWorks®, Natick, MA) and converted to NIfTI (nii) format. The T1-weighted images were used for cerebrum and cerebellum segmentation and the T2-weighted images of each mouse were used for ventricular volume segmentation with ITK-SNAP (Yushkevich et al., 2006) (www.itksnap.org).

Sensorimotor assays

All mice were evaluated on a battery of sensorimotor tests designed to assess initiation of movement (walking initiation), balance (ledge and platform), coordination (pole and inclined screens), and strength (inverted screen) using previously published methods (Grady et al., 2006; Idol et al., 2014; Wozniak et al., 2004). *Walking initiation test.* Each mouse was placed in the middle of a square outlined by white cloth tape (21 X 21 cm) on a smooth black surface of a large table top. The time it took each mouse to leave the square (place all four paws outside of the tape) was recorded. The maximum time allowed was 60 sec. *Ledge test.* Each mouse was timed for how long it could maintain its balance on a 0.75 cm wide *Plexiglas* ledge without falling (60 sec maximum). A score of 60 sec was also assigned if the mouse traversed the entire length (51 cm) of the *Plexiglas* ledge and returned to the starting

place in <60 sec without falling. *Platform test.* Each mouse was timed for how long it remained on an elevated (47 cm above the floor) circular platform (1.0 cm thick; 3.0 cm in diameter). A maximum score of 60 sec was assigned if the mouse remained on the platform for the maximum amount of time or if it could climb down on a very thin pole that supported the platform without falling. *Pole test.* A mouse was placed "head-upward" on top of a vertical rod (diameter 8 mm; height 55 cm) that had a finely textured surface. A mouse was timed for how long it took it to turn downward 180° and how long it took it to climb down the pole and reach the floor. Each mouse was given two trials with each trial lasting a maximum of 120 s. If a mouse fell from the pole before reaching the floor it was given the maximum score of 120 s. for that trial. A mean score was computed from the two trials given each animal. *60° and 90° inclined screen and inverted screen tests.* For the 60° and 90° inclined screen tests, each mouse was placed on top of an elevated (47 cm above the floor) wire mesh grid (16 squares per 10 cm) that was inclined to 60° or 90°. Each animal was placed in the middle of the screen with its head oriented down and was timed for how long it remained on the screen and how long it took to climb to the top of the screen. For the inverted screen test, mice were placed as above and then the screen was inverted to 180°. A maximum score of 60 sec was given if an animal did not fall.

Supplementary Material

Refer to Web version on PubMed Central for supplementary material.

Acknowledgments

We thank Belinda McMahan from our departmental Morphology and Imaging Core, the staff of the Mouse Genetics Core (Dr. Mia Wallace) for mice breeding and genotyping and the MRI facility (Drs. Ackerman and Garbow) at Washington University School of Medicine. The authors are grateful to Dr. Ju Chen (University of California, San Diego) for the kind gift of Nes1$^{F/F}$ mice.

FUNDING SOURCES

This work was funded by the National Eye Institute (#EY022632 to D.H.), the National Institute of Diabetes and Digestive and Kidney Diseases (#DK108005 to M.R.M), a National Eye Institute Center Core Grant (#P30EY002687), and an unrestricted grant to the Department of Ophthalmology and Visual Sciences at Washington University from *Research to Prevent Blindness*.

ABBREVIATIONS

ARCA1	Autosomal recessive cerebellar ataxia
CGN	Cerebellar granule neurons
GCL	Granule cell layer
KASH	Klarsicht/Anc1/Syne homology
KLNes1g	KASH-LESS Nesprin1 giant
MF	Mossy fibers
Nes1α	Nesprin1 alpha
Nes1β	Nesprin1 beta

Nes1g	Nesprin1 giant
NE	nuclear envelope
SYNE1	Synaptic Nuclear Envelope 1
VAGE	Vertical agarose gel electrophoresis

BIBLIOGRAPHY

Attali R, et al. Mutation of SYNE-1, encoding an essential component of the nuclear lamina, is responsible for autosomal recessive arthrogryposis. Hum Mol Genet. 2009; 18:3462–9. [PubMed: 19542096]

Baumann M, et al. Homozygous SYNE1 mutation causes congenital onset of muscular weakness with distal arthrogryposis: a genotype-phenotype correlation. Eur J Hum Genet. 2017; 25:262–266. [PubMed: 27782104]

Chambliss AB, et al. The LINC-anchored actin cap connects the extracellular milieu to the nucleus for ultrafast mechanotransduction. Sci Rep. 2013; 3:1087. [PubMed: 23336069]

Crisp M, et al. Coupling of the nucleus and cytoplasm: role of the LINC complex. J Cell Biol. 2006; 172:41–53. [PubMed: 16380439]

Duong NT, et al. Nesprins: tissue-specific expression of epsilon and other short isoforms. PLoS One. 2014; 9:e94380. [PubMed: 24718612]

Dupre N, et al. Clinical and genetic study of autosomal recessive cerebellar ataxia type 1. Ann Neurol. 2007; 62:93–8. [PubMed: 17503513]

Fanin M, et al. Dominant muscular dystrophy with a novel SYNE1 gene mutation. Muscle Nerve. 2015; 51:145–7. [PubMed: 25091525]

Grady RM, et al. Cerebellar synaptic defects and abnormal motor behavior in mice lacking alpha- and beta-dystrobrevin. J Neurosci. 2006; 26:2841–51. [PubMed: 16540561]

Gros-Louis F, et al. Mutations in SYNE1 lead to a newly discovered form of autosomal recessive cerebellar ataxia. Nat Genet. 2007; 39:80–5. [PubMed: 17159980]

Haque F, et al. SUN1 interacts with nuclear lamin A and cytoplasmic nesprins to provide a physical connection between the nuclear lamina and the cytoskeleton. Mol Cell Biol. 2006; 26:3738–51. [PubMed: 16648470]

Hodzic DM, et al. Sun2 is a novel mammalian inner nuclear membrane protein. J Biol Chem. 2004; 279:25805–12. [PubMed: 15082709]

Idol RA, et al. Neurologic abnormalities in mouse models of the lysosomal storage disorders mucolipidosis II and mucolipidosis III gamma. PLoS One. 2014; 9:e109768. [PubMed: 25314316]

Izumi Y, et al. Cerebellar ataxia with SYNE1 mutation accompanying motor neuron disease. Neurology. 2013; 80:600–1. [PubMed: 23325900]

Kobayashi Y, et al. Identification and characterization of GSRP-56, a novel Golgi-localized spectrin repeat-containing protein. Exp Cell Res. 2006; 312:3152–64. [PubMed: 16875688]

Laquerriere A, et al. Mutations in CNTNAP1 and ADCY6 are responsible for severe arthrogryposis multiplex congenita with axoglial defects. Hum Mol Genet. 2014; 23:2279–89. [PubMed: 24319099]

Loebrich S, et al. Genomic mapping and cellular expression of human CPG2 transcripts in the SYNE1 gene. Mol Cell Neurosci. 2016; 71:46–55. [PubMed: 26704904]

Mademan I, et al. Multisystemic SYNE1 ataxia: confirming the high frequency and extending the mutational and phenotypic spectrum. Brain. 2016; 139:e46. [PubMed: 27197992]

Marme A, et al. Loss of Drop1 expression already at early tumor stages in a wide range of human carcinomas. Int J Cancer. 2008; 123:2048–56. [PubMed: 18709643]

Noreau A, et al. SYNE1 mutations in autosomal recessive cerebellar ataxia. JAMA Neurol. 2013; 70:1296–31. [PubMed: 23959263]

Ozoguz A, et al. The distinct genetic pattern of ALS in Turkey and novel mutations. Neurobiol Aging. 2015; 36:1764, e9–18.

Padmakumar VC, et al. The inner nuclear membrane protein Sun1 mediates the anchorage of Nesprin-2 to the nuclear envelope. J Cell Sci. 2005; 118:3419–30. [PubMed: 16079285]

Potter C, et al. Multiple Isoforms of Nesprin1 Are Integral Components of Ciliary Rootlets. Curr Biol. 2017; 27:2014–2022. e6. [PubMed: 28625779]

Razafsky D, Hodzic D. A variant of Nesprin1 giant devoid of KASH domain underlies the molecular etiology of autosomal recessive cerebellar ataxia type I. Neurobiol Dis. 2015; 78:57–67. [PubMed: 25843669]

Razafsky D, et al. Validation of a Mouse Model to Disrupt LINC Complexes in a Cell-specific Manner. J Vis Exp. 2015:e53318. [PubMed: 26710083]

Razafsky DS, et al. Developmental regulation of linkers of the nucleoskeleton to the cytoskeleton during mouse postnatal retinogenesis. Nucleus. 2013; 4:399–409. [PubMed: 23974729]

Simpson JG, Roberts RG. Patterns of evolutionary conservation in the nesprin genes highlight probable functionally important protein domains and isoforms. Biochem Soc Trans. 2008; 36:1359–67. [PubMed: 19021556]

Sosa BA, et al. LINC complexes form by binding of three KASH peptides to domain interfaces of trimeric SUN proteins. Cell. 2012; 149:1035–47. [PubMed: 22632968]

Starr DA, Han M. Role of ANC-1 in tethering nuclei to the actin cytoskeleton. Science. 2002; 298:406–9. [PubMed: 12169658]

Stroud MJ, et al. Nesprin 1alpha2 is essential for mouse postnatal viability and nuclear positioning in skeletal muscle. J Cell Biol. 2017; 216:1915–1924. [PubMed: 28533284]

Synofzik M, et al. SYNE1 ataxia is a common recessive ataxia with major non-cerebellar features: a large multi-centre study. Brain. 2016; 139:1378–93. [PubMed: 27086870]

Uhlen M, et al. Proteomics. Tissue-based map of the human proteome. Science. 2015; 347:1260419. [PubMed: 25613900]

Volk T. Positioning nuclei within the cytoplasm of striated muscle fiber: cooperation between microtubules and KASH proteins. Nucleus. 2013; 4:18–22. [PubMed: 23211643]

Warren CM, et al. Vertical agarose gel electrophoresis and electroblotting of high-molecular-weight proteins. Electrophoresis. 2003; 24:1695–702. [PubMed: 12783444]

Wiethoff S, et al. Heterogeneity in clinical features and disease severity in ataxia-associated SYNE1 mutations. J Neurol. 2016; 263:1503–10. [PubMed: 27178001]

Wozniak DF, et al. Apoptotic neurodegeneration induced by ethanol in neonatal mice is associated with profound learning/memory deficits in juveniles followed by progressive functional recovery in adults. Neurobiol Dis. 2004; 17:403–14. [PubMed: 15571976]

Wu L, et al. Three novel recessive mutations in LAMA2, SYNE1, and TTN are identified in a single case with congenital muscular dystrophy. Neuromuscul Disord. 2017; 27:1018–1022. [PubMed: 28818390]

Yang H, et al. Generating genetically modified mice using CRISPR/Cas-mediated genome engineering. Nat Protoc. 2014; 9:1956–68. [PubMed: 25058643]

Yang J, et al. Rootletin, a novel coiled-coil protein, is a structural component of the ciliary rootlet. J Cell Biol. 2002; 159:431–40. [PubMed: 12427867]

Yoshinaga T, et al. A novel frameshift mutation of SYNE1 in a Japanese family with autosomal recessive cerebellar ataxia type 8. Hum Genome Var. 2017; 4:17052. [PubMed: 29081981]

Yucesan E, et al. SYNE1 related cerebellar ataxia presents with variable phenotypes in a consanguineous family from Turkey. Neurol Sci. 2017

Yushkevich PA, et al. User-guided 3D active contour segmentation of anatomical structures: significantly improved efficiency and reliability. Neuroimage. 2006; 31:1116–28. [PubMed: 16545965]

Zhang Q, et al. Nesprin-1 and-2 are involved in the pathogenesis of Emery Dreifuss muscular dystrophy and are critical for nuclear envelope integrity. Hum Mol Genet. 2007a; 16:2816–33. [PubMed: 17761684]

Zhang Q, et al. The nesprins are giant actin-binding proteins, orthologous to Drosophila melanogaster muscle protein MSP-300. Genomics. 2002; 80:473–81. [PubMed: 12408964]

Zhang Q, et al. Nesprins: a novel family of spectrin-repeat-containing proteins that localize to the nuclear membrane in multiple tissues. J Cell Sci. 2001; 114:4485–98. [PubMed: 11792814]

Zhang X, et al. SUN1/2 and Syne/Nesprin-1/2 complexes connect centrosome to the nucleus during neurogenesis and neuronal migration in mice. Neuron. 2009; 64:173–87. [PubMed: 19874786]

Zhang X, et al. Syne-1 and Syne-2 play crucial roles in myonuclear anchorage and motor neuron innervation. Development. 2007b; 134:901–8. [PubMed: 17267447]

Zhou X, et al. Exploring long-range genome interactions using the WashU Epigenome Browser. Nat Methods. 2013; 10:375–6. [PubMed: 23629413]

Zhou X, et al. The Human Epigenome Browser at Washington University. Nat Methods. 2011; 8:989–90. [PubMed: 22127213]

Zhou X, Wang T. Using the Wash U Epigenome Browser to examine genome-wide sequencing data. Curr Protoc Bioinformatics. 2012 Chapter 10, Unit10 10.

Zhou Z, et al. Structure of Sad1-UNC84 homology (SUN) domain defines features of molecular bridge in nuclear envelope. J Biol Chem. 2012; 287:5317–26. [PubMed: 22170055]

HIGHLIGHTS

- Expression of Nesprin1 giant is specifically abrogated in Nes1g$^{STOP/STOP}$ mice
- Nes1g$^{STOP/STOP}$ reveal the expression pattern of Nesprin1 isoforms in the cerebellum
- Nesprin1 giant associates with the ciliary rootlets of ependymal cells
- Nes1g$^{STOP/STOP}$ display enlarged ventricles
- *In vivo* evidence that ciliary Nesprin1 isoforms harbor a KASH domain

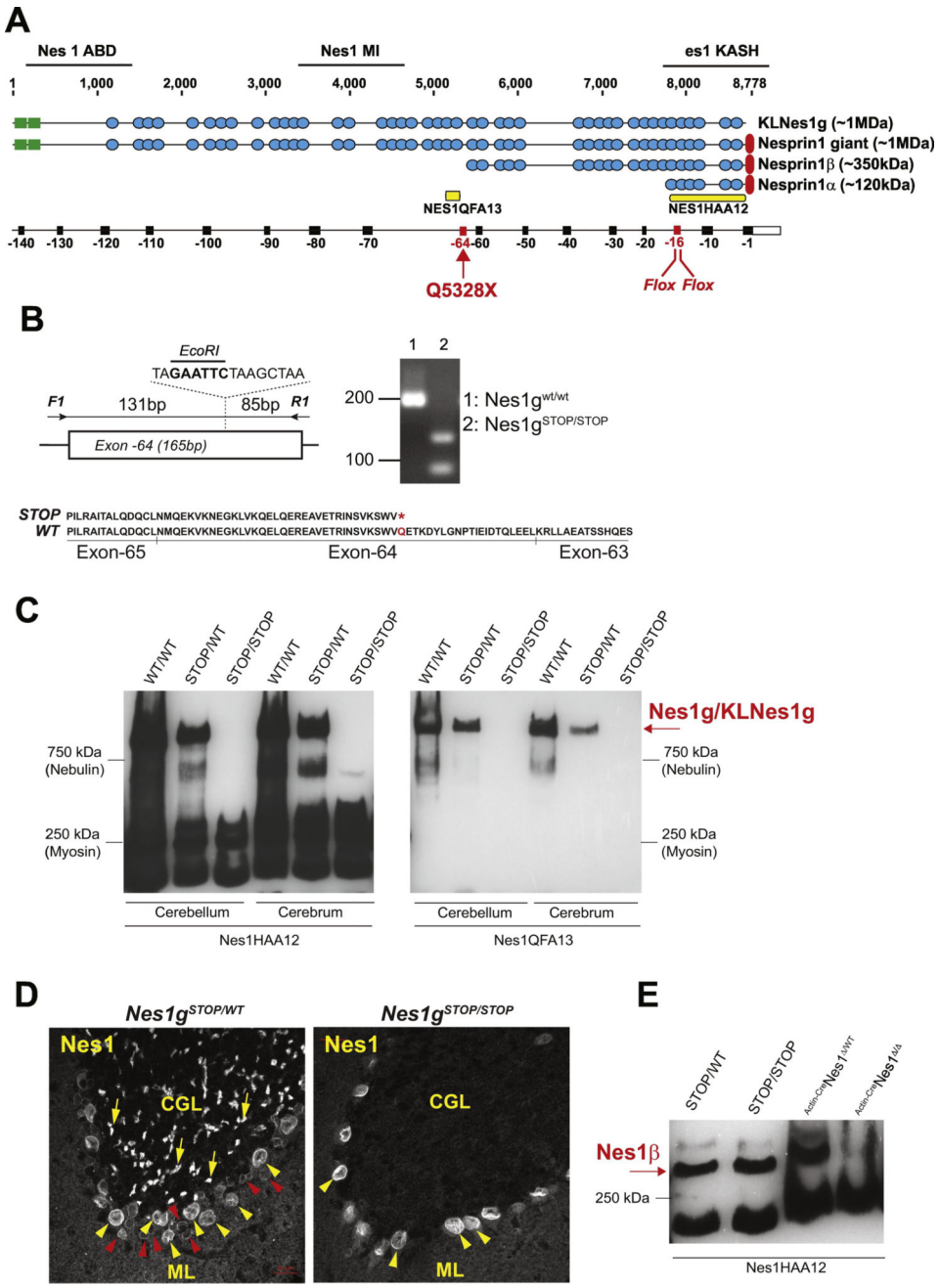

Figure 1. Development of *Nes1g*$^{STOP/STOP}$, a new mouse model of depletion of giant isoforms of Nesprin1

A) Nesprin1 isoforms (with amino acids scale, top) aligned with Syne1 exons (reverse numbering, bottom). Yellow rectangle denotes epitopes used to raise NES1QFA13 and NES1HAA12 antibodies. Q5328X denotes the nonsense mutation inserted within exon-64 upstream from the coding sequence of Nesprin1β. The floxed version of exon-16 is also indicated in red. Nes1ABD, Nes1MID and Nes1KASH refer to the position of *in situ* hybridization probes. Green rectangles: actin-binding domain; Blue circles: spectrin repeats; Red ovals: KASH domains. **B)** *Nes1g*$^{STOP/STOP}$ mice were raised through the CRISPR-Cas9-mediated insertion of 16 bases encoding STOP codons in all reading frames and

including an EcoRI restriction site for genotyping purpose. Genotyping of *Nes1g*$^{STOP/STOP}$ mice performed through EcoRI restriction of F1/R1 amplicon (216 bp) amplified from digested tails. **C)** Nes1HAA12 (left) and Nes1QFA13 (right) immunoblots of cerebellar and cerebral lysates from indicated genotypes. Note the specific loss of giant isoforms of Nesprin1 in *Nes1g*$^{STOP/STOP}$ tissues. Lysates were separated by vertical agarose gel electrophoresis (VAGE). Molecular weight markers correspond to Ponceau S-stained nebulin (750 kDa) and myosin (250 kDa) bands from skeletal muscle lysates run on the same gel. **D)** Nes1HAA12 immunofluorescence of *Nes1g*$^{STOP/WT}$ (left) and *Nes1g*$^{STOP/STOP}$ (right) cerebella. Red arrowheads: Bergmann glia; Yellow arrowheads: Purkinje cells; Yellow arrows: KLNes1g at MF/CGN synapses. GCL: granule cell layer; ML: molecular layer. Scale bars: 20 μm. **E)** Identification of the ~350 kDa Nesprin1β isoform in cerebellar lysates. Nes1HAA12 VAGE immunoblot of cerebellar lysates from indicated genotypes. Note the loss of Nesprin1β expression in cerebellar lysates from ^{ActinCre}*Nes1*$^{\Delta/\Delta}$, a mouse model of depletion of all Nesprin1 isoforms through the inducible ablation of exon-16 (Fig. 1A).

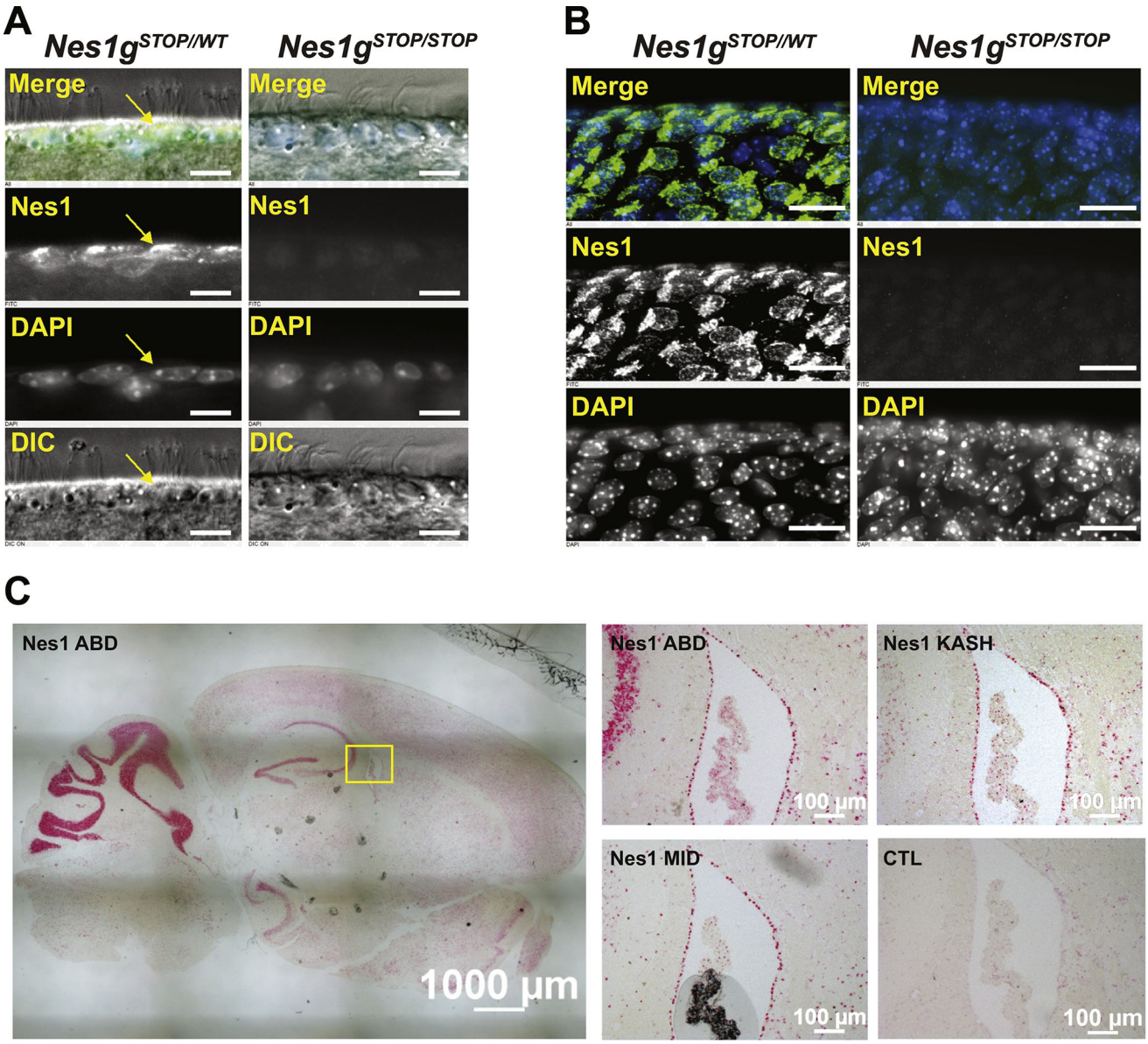

Figure 2. A giant isoform of Nesprin1 localizes to the ciliary rootlets of ependymal cells

A) Nes1HAA12 immunofluorescence of *Nes1g*$^{STOP/WT}$ (left) and *Nes1g*$^{STOP/STOP}$ (right) ependymal cells that line the ventricular lumen. Note the Nesprin1 immunoreactivity on the apical side of *Nes1g*$^{STOP/WT}$ ependymal cells (yellow arrow) just beneath ependymal cells cilia (DIC). This immunoreactivity is lost in ependymal cells of *Nes1g*$^{STOP/STOP}$ ventricles. Scale bars: 10 µm. **B)** Nesprin1 immunoreactivity at ciliary rootlets of ependymal cells viewed from the ventricular surface (see also Fig.S4) of either *Nes1g*$^{STOP/WT}$ (left) or *Nes1g*$^{STOP/STOP}$ (right) brain slices. Scale bars: 20 µm. **C)** *In situ* hybridization of consecutive C57/Bl6 brain slices showing the abundant expression of transcripts recognized by probes annealing to the 3' (Nes1ABD), middle (Nes1MID) and 5' (Nes1KASH) region of Nesprin1giant transcripts in ependymal cells lining brain ventricles. CTL: same experiment performed with a bacterial control probe (dapB).

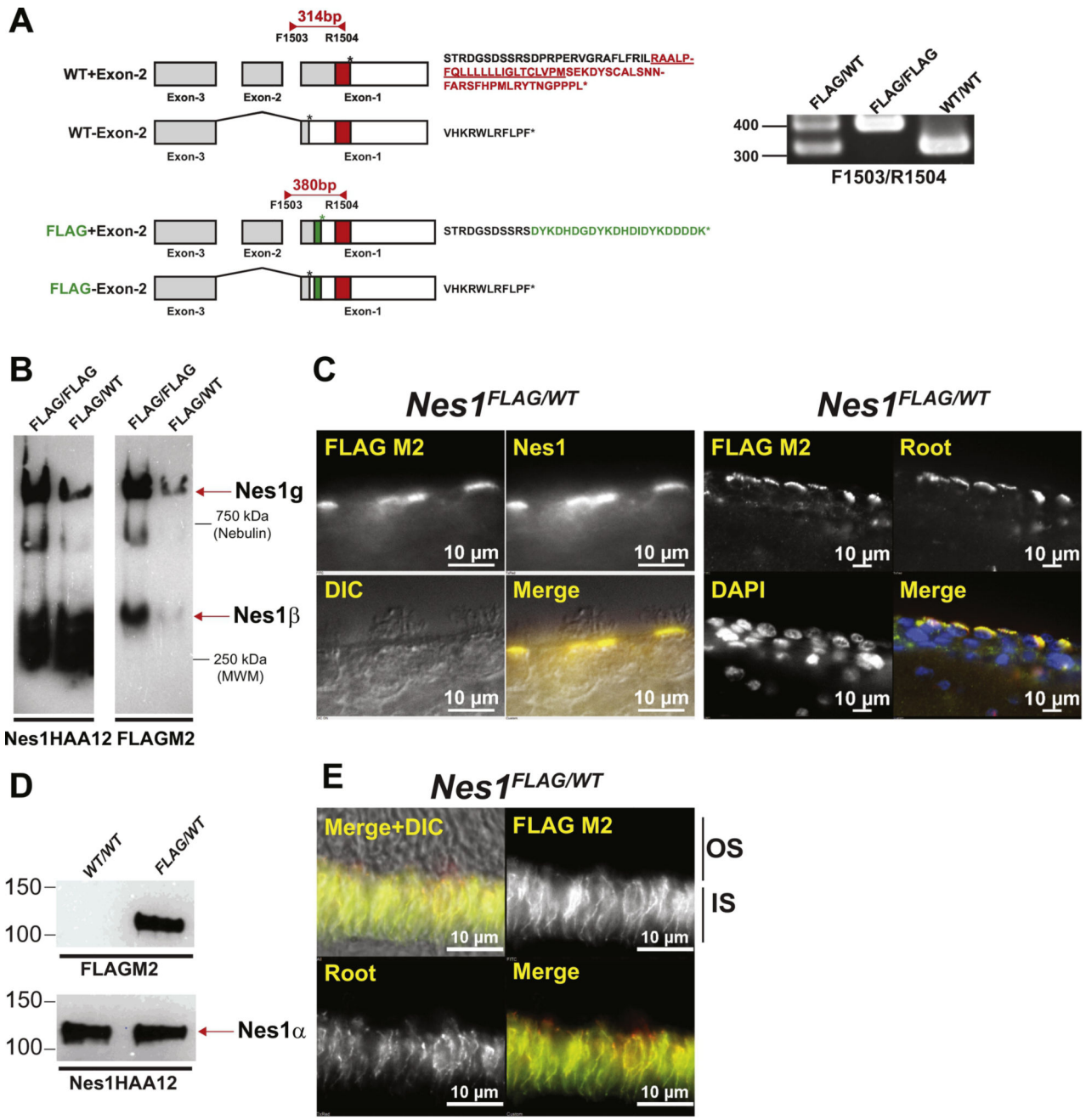

Figure 3. The giant ciliary isoform of Nesprin1 harbors a KASH domain

A) Genetic strategy used to swap the C-terminal KASH domain of Nesprin1 with a 3XFLAG/STOP epitope. *Top*: C-terminal amino acid sequences of natural Nesprin1 isoforms resulting either from the inclusion (WT+exon-2, KASH domain in red with underlined transmembrane domain) or the splicing (WT-exon-2, leading to a frameshift of exon-1 and encoding KASH-LESS isoforms) of exon-2 within *Syne1* transcripts. *Bottom*: C-term sequences of recombinant Nesprin1 isoforms synthesized from alleles harboring a 3XFLAG insertion followed by a STOP codon in frame and upstream from the coding sequence of the KASH domain. Note that in 3XFLAG transcripts that retain exon-2 (FLAG

+exon-2), the C-term KASH domain is replaced by a C-term 3XFLAG tag. By contrast, 3XFLAG transcripts that do not include exon-2 still encode natural KASH-LESS isoforms. Red rectangles: coding sequence of the KASH domain. Green rectangles: coding sequence of 3XFLAG. *: STOP codons. Coding sequences and 3'UTR are in grey and right, respectively. *Right*: genotyping of FLAG-tagged alleles with F1503 and R1504 primers. 380 bp amplicons are indicative of the insertion of the 3XFLAG-STOP sequence (66bp). **B)** Nes1HAA12 (left) and FLAGM2 (right) immunoblots of Nes1$^{FLAG/FLAG}$ and Nes1$^{FLAG/WT}$ cerebral lysates separated by VAGE. Note that all FLAGM2-immunoreactive bands comigrate with Nes1HAA12-immunoreactive bands that correspond to giant isoforms of Nesprin1 and to Nesprin1β. **C)** Colabeling of Nes1$^{FLAG/WT}$ brain slices with FLAGM2 and either NES1HAA12 (left) or rootletin (right). **D)** FLAGM2 (top) and NES1HAA12 (bottom) immunoblots of retinal lysates from Nes1$^{WT/WT}$ and Nes1$^{FLAG/WT}$ littermates. Note the FLAG-tagged band that is specifically detected in Nes1$^{FLAG/WT}$ lysates and comigrates with Nes1α (120 kDa). **E)** FLAGM2 and rootletin colabeling of Nes1$^{FLAG/WT}$ retinas. Note the FLAGM2 immunoreactivity that colocalizes with the ciliary rootlets that line the inner segment (IS) of photoreceptors. OS: outer segments of photoreceptors.

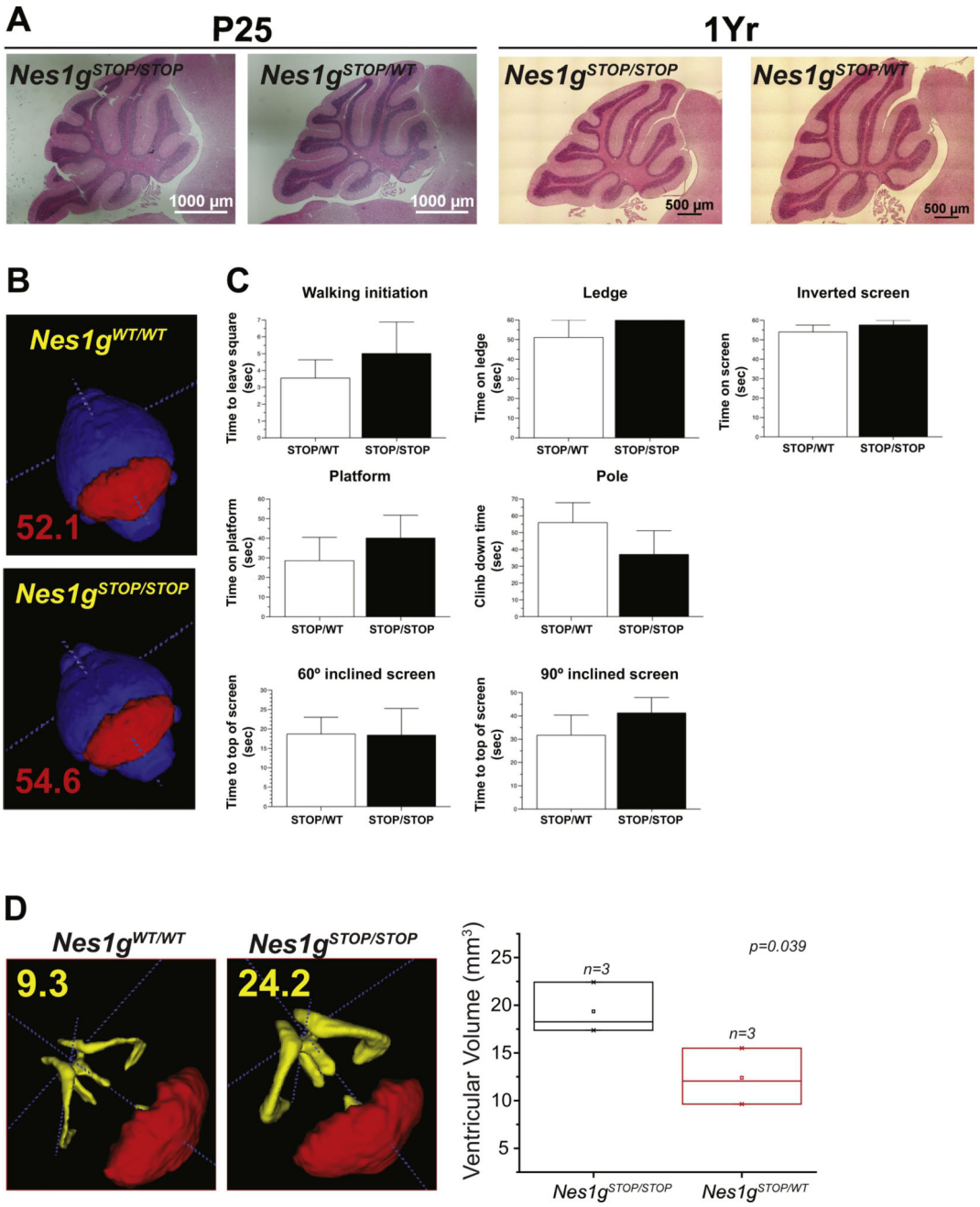

Figure 4. ***Nes1g*$^{STOP/STOP}$ mice do not recapitulate the cerebellar pathologies of *SYNE1* patients but display enlarged ventricles**

A) Hematoxylin and Eosin staining of P25 and 1 year-old cerebella from indicated genotypes. **B)** 3D rendering of cerebellar volumes (red) following segmentation of MRI scans of 1 year-old *Nes1g*$^{WT/WT}$ (top) and *Nes1g*$^{STOP/STOP}$ (bottom) brains. Cerebellar volumes (in mm^3) are indicated. **C)** Behavioral analysis of *Nes1*$^{STOP/WT}$ (white) and *Nes1g*$^{STOP/STOP}$ (black). No statistical difference (n=4 for each genotype) was observed in any of the indicated tests. **D)** *Left*: 3D rendering of ventricular volumes of 1 year-old *Nes1g*$^{WT/WT}$ (left) and *Nes1g*$^{STOP/STOP}$ (right). Ventricular volumes (in mm^3) are indicated.

Right: ventricular volumes of ~3 month-old *Nes1g*$^{STOP/STOP}$ and *Nes1g*$^{STOP/WT}$ mice (n=3 for each genotype).